



Tribological behavior of glass fiber reinforced-PA66 in contact with carbon steel under high contact pressure, sliding and grease lubricated conditions

Takeshi Kunishima, Yasuharu Nagai, Takanori Kurokawa, Gaëtan Bouvard,
Jean-Christophe Abry, Vincent Fridrici, Phillippe Kapsa

► To cite this version:

Takeshi Kunishima, Yasuharu Nagai, Takanori Kurokawa, Gaëtan Bouvard, Jean-Christophe Abry, et al.. Tribological behavior of glass fiber reinforced-PA66 in contact with carbon steel under high contact pressure, sliding and grease lubricated conditions. *Wear*, 2020, 456, pp.203383 -. 10.1016/j.wear.2020.203383 . hal-03492133

HAL Id: hal-03492133

<https://hal.science/hal-03492133>

Submitted on 18 Jul 2022

HAL is a multi-disciplinary open access archive for the deposit and dissemination of scientific research documents, whether they are published or not. The documents may come from teaching and research institutions in France or abroad, or from public or private research centers.

L'archive ouverte pluridisciplinaire **HAL**, est destinée au dépôt et à la diffusion de documents scientifiques de niveau recherche, publiés ou non, émanant des établissements d'enseignement et de recherche français ou étrangers, des laboratoires publics ou privés.



Distributed under a Creative Commons Attribution - NonCommercial 4.0 International License

Tribological behavior of glass fiber reinforced-PA66 in contact with carbon steel under high contact pressure, sliding and grease lubricated conditions

Takeshi Kunishima ^{a, b}, Yasuharu Nagai ^a, Takanori Kurokawa^a, Gaëtan Bouvard ^b, Jean-Christophe Abry ^b, Vincent Fridrici ^b, Phillippe Kapsa ^b

^a JTEKT CORPORATION, 333 Toichi-cho, Kashihara, Nara 634-8555, Japan

^b Laboratoire de Tribologie et Dynamique des Systèmes, UMR CNRS 5513, Ecole Centrale de Lyon, Université de Lyon-36 avenue Guy de Collongue F-69134 Ecully cedex, France

Corresponding author: Takeshi Kunishima E-mail: takeshi_kunishima@jtekt.co.jp

Keywords: Polyamide, Glass fibers, Wear, Grease, Composite, Worm gear

ABSTRACT

Polyamide 66 is widely used for sliding parts, such as resin worm gear. Glass fibers are usually added to increase its strength. In this study, the tribological behavior of glass fiber reinforced-polyamide 66 composite in contact with carbon steel under high contact pressure, sliding, and grease lubricated conditions is studied. Measurement of mechanical properties and SEM observations of composite sliding surfaces after different sliding cycle numbers indicate that sliding induces characteristic damage of the surface (peeled off fibers and scratching of polyamide) and a degradation in mechanical properties. These lead to an increase in friction and creep of the composite. The wear effect increases with the increase in sliding cycles, and the initial orientation of the fibers in the composite sliding surface has significant effects on the wear of the steel counterpart. The contribution of each phenomenon to the tribological behavior is discussed. The damage to the composite surface and the increase in contact temperature due to sliding have great effects on the tribological properties compared to the presence of wear debris in grease and wear on the steel. The effects of the hardness of the steel on the tribological properties are investigated, and it is found that wear of the composite is reduced by using softer steels.

1. Introduction

The requirements for lighter automobile resin parts to achieve energy savings and to reduce carbon dioxide emissions are increasing owing to energy issues such as global warming. In addition, the use of resin-made sliding parts in the automotive industry is increasing in response to the demand for higher levels of quiet accompanying the computerization and hybridization of automobiles [1-4]. Among various types of resin materials, polyamide 66 (hereinafter PA66) is known as an engineering plastic, and has useful properties, such as heat resistance, high strength, toughness, and high wear resistance [5-8]. Therefore, PA66 is widely used for sliding parts in automobiles or industrial machines such as various types of gears [9-13], bearing retainers [14-16], and rollers [17]. Recently, the requirements for the downsizing of automobiles and industrial machines and growing concern for the environment have increased the demand for reducing the size and weight of these

plastic sliding parts and their capability to withstand high stress [18, 19].

The demand for the use of plastic worm gears is particularly important in the worm reducer of the automobile electric power steering because the gears are lightweight, reduce vibration and noise, and are corrosion resistant. The plastic worm gear of the reducer used in electric power steering experiences a significantly high contact pressure (over 100 MPa) under sliding conditions. Therefore, some form of grease lubrication is necessary to reduce friction between the plastic worm gear and the steel worm shaft [20-22]. In this application, the effect of sliding is greater than the effect of rolling. The recent downsizing of automotive components, coupled with the high demand for electric power steering in large vehicles owing to their impact on fuel economy, highlights the need for robust worm gear support. However, applying higher torque to worm gears will lead to large deformation of the teeth of the plastic gear (increase in the backlash), breakage at a much earlier stage, and increase of the sliding torque [23].

As a consequence, improvements in the mechanical properties of plastic materials are required. Adding reinforcement fibers, such as glass fibers (GF), carbon fibers (CF), or aramid fibers (AF), is a common means to improve the tribological properties of polyamide [24-29]. Kim et al. [27] noted that adding GF can decrease the friction coefficient and wear amounts of polyamide 12 material by decreasing the adhesion between polyamide 12 and carbon steel under dry conditions; the lowest friction coefficient and a better wear resistance of polyamide 12 composite were achieved at 30 wt% addition of GF. In addition, they noted that fibers in a parallel orientation exhibited slightly higher friction levels than those in a perpendicular orientation. However, the fiber orientation had less effect on the friction and wear of the composite than the fiber content or the applied load. Shin et al. [28] found that the amount of GF in the composite and the molecular weight were strongly affected by the friction level and the wear rate because these altered the shear strength and adhesion of PA66 when performing block-steel ring sliding tests under dry conditions. They also stated that the temperature at the sliding interface was important in determining the morphology of the wear debris, which was closely related to the wear resistance. Kim et al. [29] demonstrated that the wear resistance of unreinforced PA66 and GF reinforced PA66 became worse with water absorption because of softening caused by absorbed water and increased interfacial adhesion on the steel counter surface. In addition, the degraded wear characteristics of unreinforced PA66 resulting from chain scission of the amide functional group caused by water molecules were substantially improved by using short-GF reinforcement.

The majority of the previous studies on the tribology of fiber reinforced polyamide were performed in dry conditions, and there are very few reports on the tribological properties of fiber reinforced PA66 under grease lubrication. The reason is that polymer materials have self-lubricating properties, and it is possible to use them as sliding parts without lubrication in many cases. Kurokawa et al. [30] reported that the tribological properties of spur gear made using CF-reinforced polyamide 12 material improved under grease lubrication, and that the load bearing characteristic was higher with increasing molecular weight of polyamide 12. However, the counterpart gear was made of the same polyamide 12 material. In addition, they reported that increasing the molecular weight of polyamide 12 can improve the fatigue properties of resin gear. However, few explanations were provided regarding the wear mechanism of the composite material. Kurokawa et al. [31] further reported on the tribological properties of spur gear made from CF-reinforced PEEK (poly-ether-ether-ketone) under

lithium grease lubrication, with a counterpart of CF-reinforced PEEK or steel. They stated that the affinity between PEEK and CF, the difference in the intervention of CF worn debris at the engagement region, and the characteristics of CF (strength and modulus of fibers) play a significant role in determining the wear resistance of the composite. Kunishima et al. [32] reported on the tribological properties of carbodiimide-added GF and AF-reinforced PA66 in contact with steel in the presence of Ba complex grease. They stated that the toughness and wear resistance of the PA66 composite were improved by the increase of the molecular weight of PA66 through the reaction extrusion between PA66 and poly-carbodiimide compounds. However, the detailed tribological mechanism of the composite and steel counterpart was not discussed.

It is necessary to consider not only the wear resistance of PA66 but also the wear resistance of the metallic counterpart, especially when using hard-fiber reinforced PA66 material, which may have the most aggressive effects on the metallic counterpart because the wear on both materials will lead to much earlier breakage of actual parts and to an increase of the sliding torque. However, the wear mechanism has not been clarified sufficiently. Particularly, considering an actual worm gear, the machining of the teeth and the heat treatment of the steel worm shaft affect the performance of the products and their production costs. For example, applying a heat treatment to the steel worm shaft counterpart before the formation of the teeth will make the formation of the teeth much more difficult, leading to increased production costs. On the other hand, if the heat treatment of the worm shaft is applied after the formation of the teeth, the accuracy of the dimensions of the worm shaft decreases because of the strain induced by the heat treatment, and the gear meshing accuracy will decrease, leading to undesirable effects on the product's performance. Therefore, it is necessary to understand the tribological phenomena to properly design the contact surface of the composite and to select the proper steel and grease. A previous study on the effects of the metallic counterpart on the tribological properties of fiber reinforced-PA66 by Chen et al. [33] found that the type of metallic counterpart (such as aluminum, brass, or steel with different surface treatment or heat treatment) has notable effects on the wear resistance of GF-reinforced PA66 and on the friction coefficient during the rolling-sliding contact. They indicated that this difference was attributed to the capability of the metal surface to form a stable polymer transfer film, and that the surface treatment for steel (such as Tufftride coating) has a significant effect on the wear rate of GF-reinforced PA66. However, all sliding tests were performed in dry conditions, and the effect of the hardness of steel was not investigated in their study.

Given these points, the present study focuses on the typical tribological properties during sliding of GF-reinforced PA66 and a steel counterpart under high contact pressure and grease lubricated conditions (i.e., the wear resistance of GF-reinforced PA66 and steel, and the associated friction properties). First, the change over time of the tribological properties is investigated, and the contribution of each parameter such as the damage in the sliding surface, the contamination by wear debris in the grease, and the increase of surface temperature on the tribological properties are elucidated. The wear resistance of the steel counterpart is discussed, considering the fiber orientation of the composite sliding surface. Furthermore, the effects of the mechanical properties of the steel counterpart on the tribological behavior are evaluated.

2. Experimental

2.1 Experimental set-up, measurement, and observation

Tribological properties were evaluated through sliding tests under grease-lubricated conditions using a rotating composite ring in contact with four fixed steel cylinders [23, 32]. Figure 1 presents the schematic view of the test specimens used for the sliding test as well as the tribometer setup. With this test setup, it is possible to perform sliding tests under high-contact pressure and sliding conditions, similar to those encountered by commercial worm gears. Intermittent sliding, in which rotation and stopping periods are alternated, was introduced to reduce excessive sliding heat generation. The sliding tests were carried out under lubricated conditions with 0.85 g of grease used for each sliding test. A normal load was applied using dead weights. The weight and height of each composite ring specimen were measured before and after each sliding test to estimate the wear and the creep separately, and to investigate the contributions of wear and creep in a sample. The total height loss h_{total} is the total loss caused by wear and creep, while the wear height loss h_{wear} can be calculated from the wear rate of the composite M_{wear} , the density of the composite $d = 1.23 \text{ g/cm}^3$, and the sliding surface area s (approximately 200 mm^2) using the following equation.

$$h_{wear} = \frac{M_{wear}}{ds} \quad (1)$$

The creep height loss h_{creep} was then estimated by subtracting the wear height loss from the total height loss.

$$h_{creep} = h_{total} - h_{wear} \quad (2)$$

In addition, the vertical displacement was measured in situ during the sliding tests. However, this value was not exactly the same as the height loss of the composite ring measured before/after sliding tests because the composite ring specimens expanded because of the heat generated by sliding during the tests and then contracted because of cooling after each test. In our tests, the temperature of the steel cylinder holder was measured with a thermocouple. The friction torque F was measured with a friction torque sensor, and the friction coefficient μ was calculated using the normal load N and rotation radius r (11.4 mm).

$$\mu = \frac{F}{rN} \quad (3)$$

Friction torque was measured every 0.01 s, and the average value and maximum value of the friction coefficient calculated in 1 s increments. One cycle in this sliding test represents one rotation of the composite ring. Table 1 lists the sliding test conditions. The sliding surfaces of the composite ring were observed before and after each sliding test with a microscope and using scanning electron microscopy (SEM). The mass losses of individual steel cylinders were measured, and wear scars were observed using interferometry. The Young's modulus of the composite sliding surface and hardness of the sliding surface of the steel cylinder were measured through micro

indentation. Table 2 presents the measurement conditions.

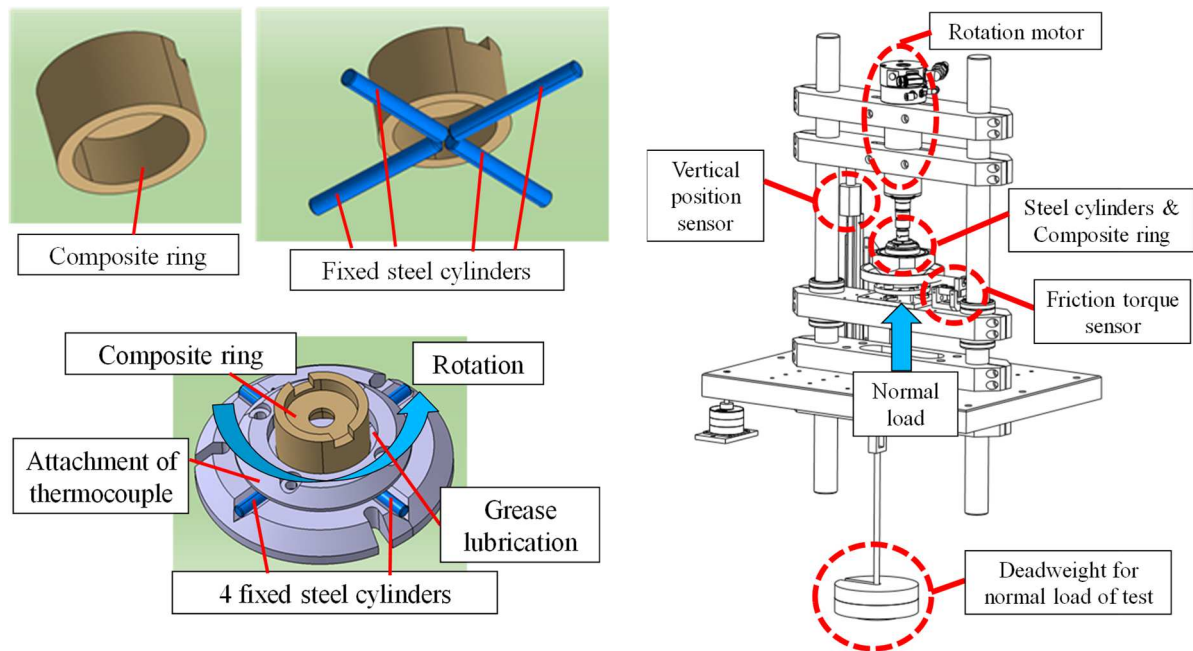


Fig. 1 Schematic view of test specimens and sliding test setup

Table 1 Test conditions for the sliding tests

Steel cylinders (x4)	Diameter	3.5 mm
	Length	30 mm
	Material	Carbon steel
	Young's modulus	205 GPa
Composite ring (JIS K 7218)	Outer diameter	25.6 mm
	Inner diameter	20 mm
	Height	12 mm
Test conditions	Mean rotation speed	790 rpm (Radius of rotation: 11.4 mm)
	Mean sliding speed	1 m/s
	Normal load	350 N
	Contact pressure	198 MPa (at 25 °C)
	Test time	12–88 min: intermittent process (10 s sliding and 1 s stopping)
	Cycles	1,900 – 61,500
	Environment temperature	25 °C

	Lubrication	Grease
--	-------------	--------

Table 2 Micro indentation test conditions.

Measured sample	Composite ring	Steel cylinder
Type of indenter	Vickers	Vickers
Maximum normal load	1,500 mN	300 mN
Indentation test procedure	Load: 0→1,500 mN for 10 s Creep: 1,500 mN for 5 s Unload: 1,500 mN ⇒ 40 mN for 4 s	Load: 0→300 mN for 10 s Creep: 300 mN for 5 s Unload: 300 mN ⇒ 40 mN for 4 s

2.2 Composite material

Commercially available raw materials were extruded to fabricate pellets (granules). Test specimens were then fabricated through injection molding of the pellets. Unreinforced PA66 pellets were used as the raw PA66 material. GF were cut to the desired length for use (fiber diameter: 6.5 μm , length: 3 mm). The chopped GF strands were treated with an agent to ensure good adhesion between the PA66 and GF (details: see Supplementary Figure S1). The extrusion of PA66 and GF chopped strands was carried out by using a twin-screw extruder (TEM-26SX, Toshiba Machine Co., Ltd.). PA66 was fed into the top feed (i.e., fed from the root of the barrel of the twin screw extruder), while fibers were fed into the side feed (i.e., fed from the middle of the barrel of the twin screw extruder) to prevent damage of fibers during extrusion and to ensure the length of the fibers was maintained inside the pellets. The amount of GF was 15 wt%. After extrusion, injection molding was carried out with an injection molding machine (ROBOSHOT S-2000i 100B, FANUC CORPORATION), and the sliding test specimens described in Section 2.1 were prepared. The viscosity number, which is related to the molecular weight of PA66, was measured using the relative viscosity method with a formic acid solvent at 25 °C, according to the ISO307 standard. The viscosity of the test specimens was 145 ml/g, which falls within the normal level of the molecular weight of PA66.

The composite ring specimens were cut in the height direction by 3 mm with a lathe, and then the sliding surface was polished with #600 polishing paper before each sliding test. The objective of this process was to simulate the conditions of the sliding surface of actual worm gear tooth surfaces, which are formed by mechanical hob-cutting after the injection molding process to ensure dimensional stability (see Supplementary Figure S2).

2.3 Steel cylinders

Steel cylinders with a diameter of 3.5 mm and length of 30 mm were fabricated using S45C steel, which contains 0.45 % carbon, following JIS G 4051 (Japanese Industrial Standards). The roughness of the sliding surface was Ra 0.2 μm , obtained using a centerless grinding process. In addition to the raw carbon steel, cylinders with different hardness and metal structure were prepared by applying different heat treatment

processes (quench hardening and tempering), as presented in Figure. 2. First, the same types of carbon steel cylinders with a diameter of 3.6 mm were prepared and heat treatments under different conditions were applied. Afterward, each sample was machined to a diameter of 3.5 mm using the same process to obtain the same roughness (R_a of 0.2 μm). Table 3 presents the heat treatment conditions and the measured hardness of the cylinders measured in the way described in Section 2.1 (steel structure: see Supplementary Figure S3).

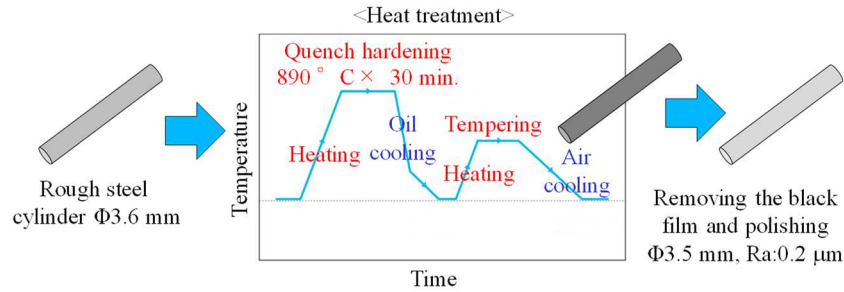


Fig. 2 Heat treatment process of steel cylinder.

Table 3 Heat treatment conditions for steel cylinders. Values of the hardness are the average values for 5 measurements.

Quench hardening	Tempering	Hardness measured by micro indentation
- (Raw steel)	-	4.5 +/- 0.1 GPa
890 °C × 30 min. Oil cooling	412 °C×60 min. Air cooling	5.4 +/- 0.2 GPa
	300 °C×60 min. Air cooling	7.2 +/- 0.1 GPa
	120 °C×60 min. Air cooling	9.9 +/- 0.2 GPa

2.4 Grease

The base oil of the evaluated grease was PAO8 (Polyalphaolefin 8) and the thickener consisted of urea compounds. The grease contained zinc carboxylate acting as a low-friction agent and contained a sulfur type anti-oxidation agent.

3. Results and Discussion

3.1 Detailed tribological behavior of the contact and damage of the composite

Figure 3 shows the evolutions of the vertical displacement, the temperature, and the average friction coefficient (μ) during 61,500 cycles for a normal load of 350 N and a stopping time of 1 s (after every 10 s of sliding), with the steel cylinders (hardness: 4.50 GPa). The temperature of the sliding surface was increased from 25 °C to 102 °C. The displacement did not increase in the initial stage of the test (indicating that neither wear nor creep occurred) and the average friction coefficient was 0.035–0.045. Example of the evolution of the friction coefficient for 2 s from the restart of the sliding after stopping phase are shown in Supplementary Figure S4. After the initial stage (around 21,000 cycles), both the maximum friction coefficient and average friction

coefficient started to increase, as presented in Figure. 4 (before the increase of the vertical displacement), and then an increase of the vertical displacement of 0.1 mm was observed (inflection point of vertical displacement). At the inflection point, the slope of the temperature increased, which is related to the increase of the friction coefficient. Afterward, a steady state displacement was observed, and then the displacement began to increase proportionally to the number of cycles. The sliding tests were performed under the same conditions using the same materials seven times, and the first inflection point of the vertical displacement ranged between 19,000 cycles and 23,000 cycles. Figure 5 presents each test specimen and grease before and after the sliding test of 61,500 cycles, as observed by microscope. The entire sliding surface of the composite ring was damaged, and the sliding surface was expanded in both inner and outer directions; this indicated that both wear and creep occurred during sliding. The sliding surface of the steel cylinder was worn severely (exhibiting scratches) in the sliding direction, indicating that 2-body abrasive wear occurred. The total wear volume of the four steel cylinders after 61,500 cycles was 0.158 mm^3 and was less than 112 mm^3 , which was the wear volume of the composite ring after 61,500 cycles. In addition, the color of the grease changed from a light color to black. Figure 6 shows the wear debris inside the grease after a sliding test. The image was obtained by centrifugation of the grease to separate the base oil and then heating the residue to evaporate any organic agents (such as thickeners). The presence of fibers can be observed in the wear debris. In addition, the elements related to GF (Si, Al) and carbon steel (Fe) were detected by SEM-EDX analysis of the wear debris in the grease (images in Supplementary Fig.S5).

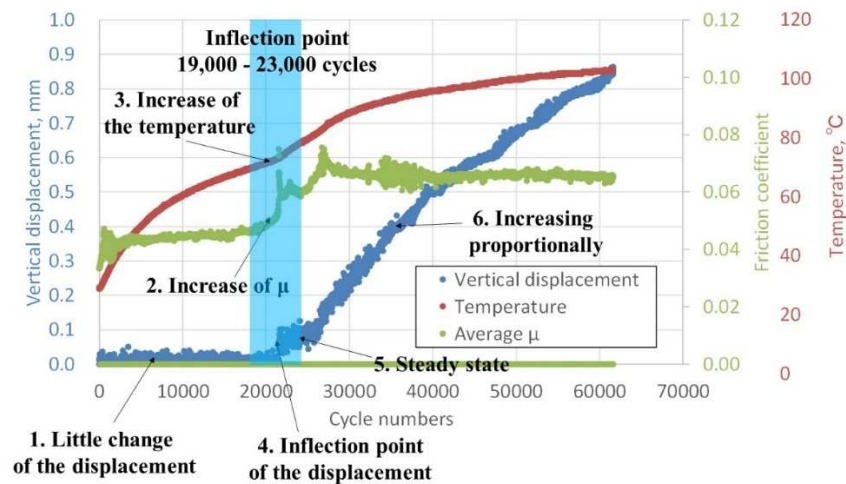


Fig. 3 Test chart over 61,500 cycles.

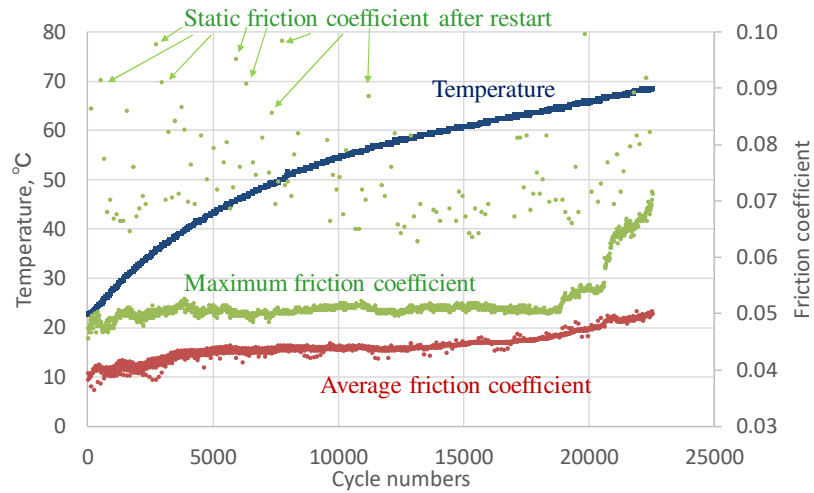


Fig. 4 Evolution of the temperature and the friction coefficient before the inflection point of the vertical displacement.

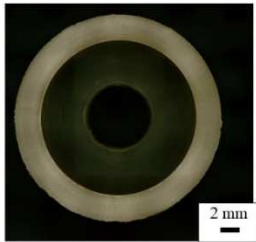

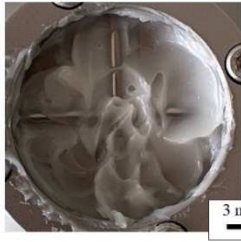
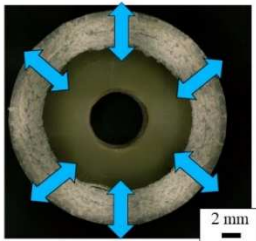

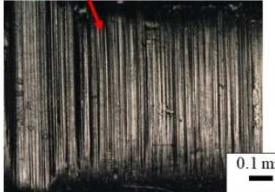

	Composite ring	Steel cylinder	Grease
Before sliding test			
After sliding test	 Wear amount of composite: 0.14 g Wear volume: 112 mm ³ Height decrease: 0.82 mm	  Wear volume: 0.158 mm ³ (Total of 4 cylinders)	

Fig. 5 Test specimens and grease before/after the sliding test (observed by optical microscope).

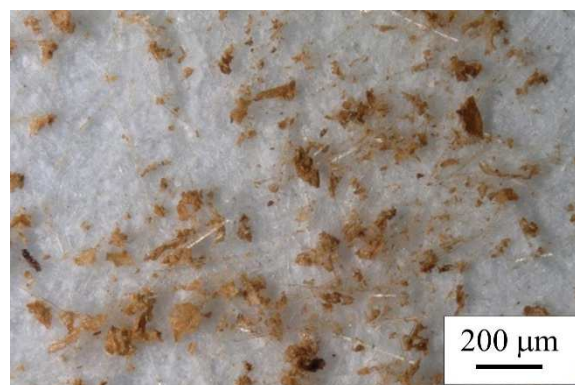


Fig. 6 Optical microscope image of wear debris in grease.

To clarify the reasons for the first inflection point of the vertical displacement and to estimate the ratio of wear and creep in each stage, eight individual tests with different cycle numbers were performed. Figure 7 shows the absolute value of the wear and the creep represented by the total height loss, and the calculated ratio of wear and creep for each cycle. There was good correlation between the creep as estimated by the calculation explained in Section 2.1 and the surface area after the sliding tests (measured with the optical microscope), which is supposed to be directly related to the creep of the composite ring (see Supplementary Figure S6). In the initial stage of the sliding test (in other words, in the first inflection point of the vertical displacement), the height decrease was mainly due to creep; however, the effects of wear started to increase after the first inflection point, and in the last stage of the sliding test, the main factor contributing to height loss was wear. The process involving wear and creep during the sliding tests was clarified by detailed observations as follows.

Figure 8 shows the optical microscope observation of the sliding surface of the composite ring at different cycles. At 10,000 and 17,000 cycles, partial peeling of the sliding surface has already occurred, especially in the center region. By contrast, at 22,531 cycles (just before the inflection point of the vertical displacement for this test), the peeling of the center area of the sliding surface was advanced. The reason why the peeling of the composite was promoted especially in the center area will be explained in Section 3.2 by considering the fiber orientation at the sliding surface of the composite ring. In the sample tested for 19,995 cycles (just after the inflection point for this test), peeling of the center area of the sliding surface was observed. From then on, peeling spread across the entire sliding surface. To discuss the damage of the sliding surface quantitatively, the mechanical properties of the sliding surface were measured by micro indentation. Using this method, the size of the indentation after a measurement was approximately 100 μm . Therefore, the mechanical properties of not only the fibers and the PA66 itself, but also the composite itself, can be discussed. Figure 9 presents the obtained Young's modulus in an area without peeling (no-peel area) and a peeled area for each cycle. In the no-peel area, the value was almost the same as a new sample until 17,000 cycles, and decreased slightly up to 22,531 cycles. By contrast, the Young's modulus decreased compared to the initial conditions even at 10,000 and 17,000 cycles in the peeled area, and by 22,531 cycles, the value had decreased significantly. Considering these results, the damage to the sliding surface was related to the mechanical properties in a quantitative manner.

Figure 10 presents the SEM observation of the sliding surface of the composite ring at different cycles. SEM observations were performed under the BSE (backscattered electron) mode, where the white area is the GF and the gray area is the PA66. After 10,000 cycles, small holes in the PA66 are observed. However, GF adhered to PA66 correctly and severe damage is not observed. At 17,000 cycles, additional damage is observed; holes where the GF had fallen off the sliding surface were observed, and scratches of the sliding surface related to the missing GF are observed. At 22,531 cycles (just before the inflection point of the vertical displacement in this test), even in an area where severe peeling was not present (observed with the optical microscope), peeling off of GF, damage to GF, and wear debris from the steel are confirmed. In addition, some scratches are observed in the sliding direction.

Considering these mechanical properties and the observations made using a microscope and SEM, the friction coefficient is considered to have increased owing to the damage incurred by the sliding surface, and initial creep

was induced by the decrease in the mechanical properties of the composite due to the peeling off of GF. Afterward, the GF dropped off continuously from the sliding surface and further wear was promoted as the sliding cycles increased in number.

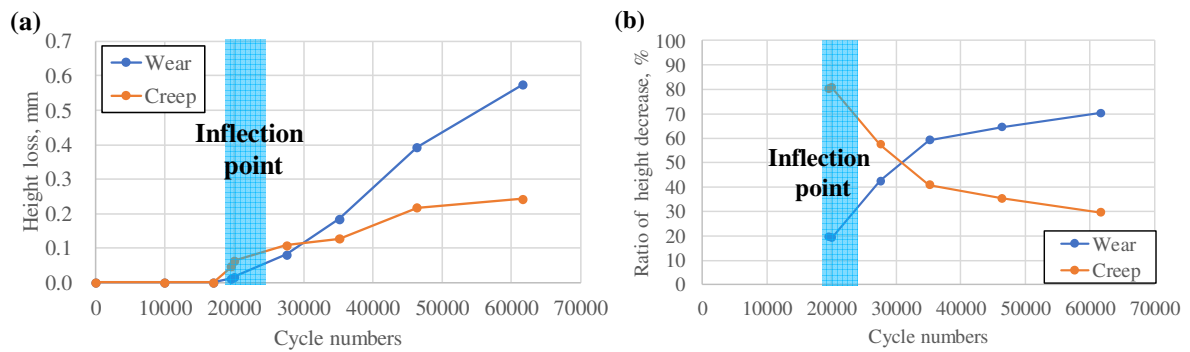


Fig. 7 (a) Height loss representing wear and creep at different cycles and
(b) height loss ratio due to wear and creep

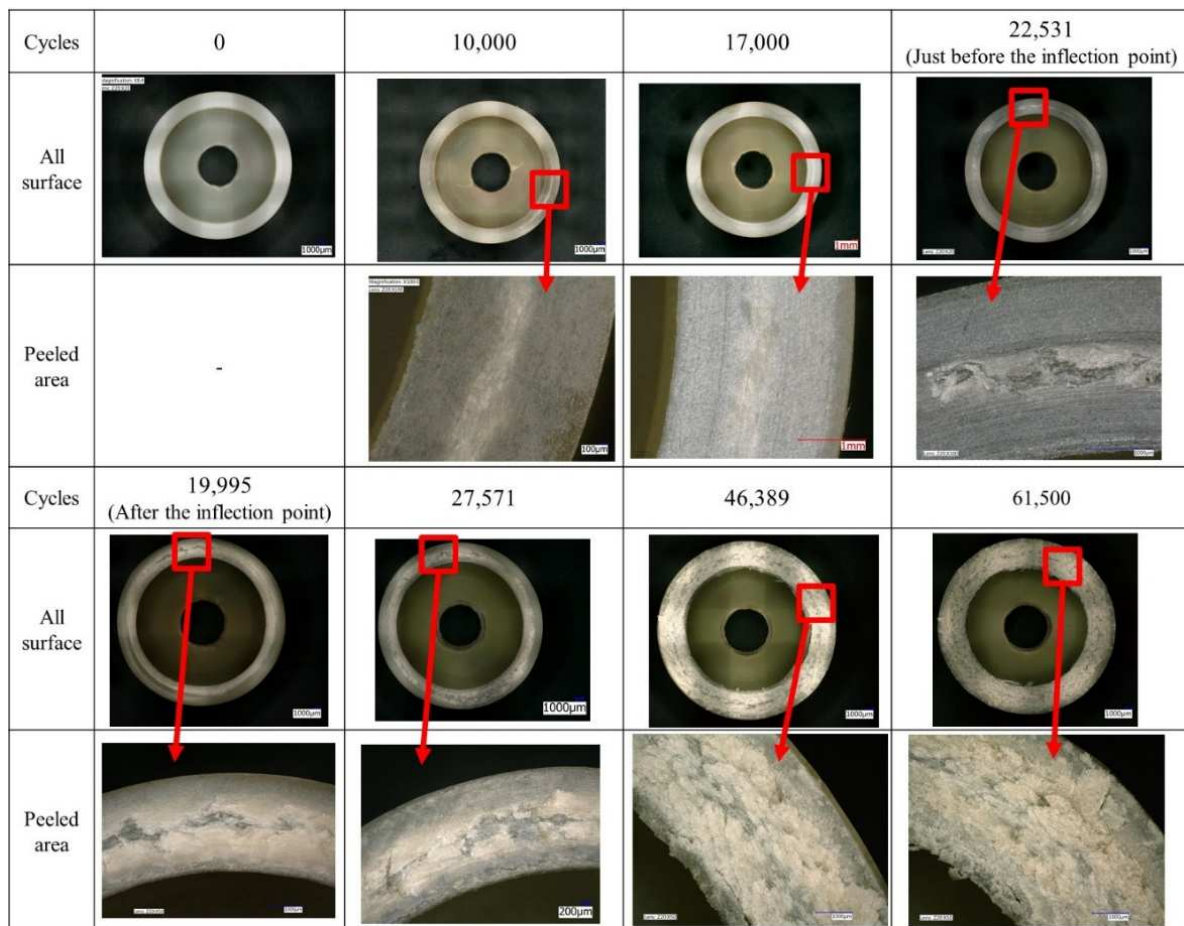


Fig. 8 Optical microscope observations of the sliding surface of composite rings for various test durations.

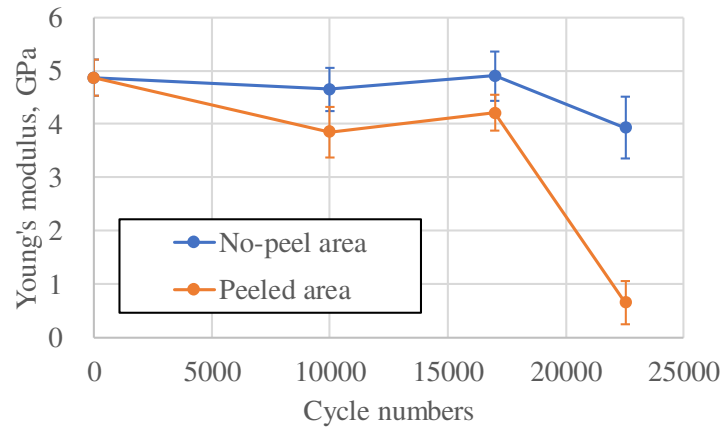


Fig. 9 Young's modulus of the sliding surface of the composite ring at different cycles (measured by micro indentation, average values of 5 measurements).

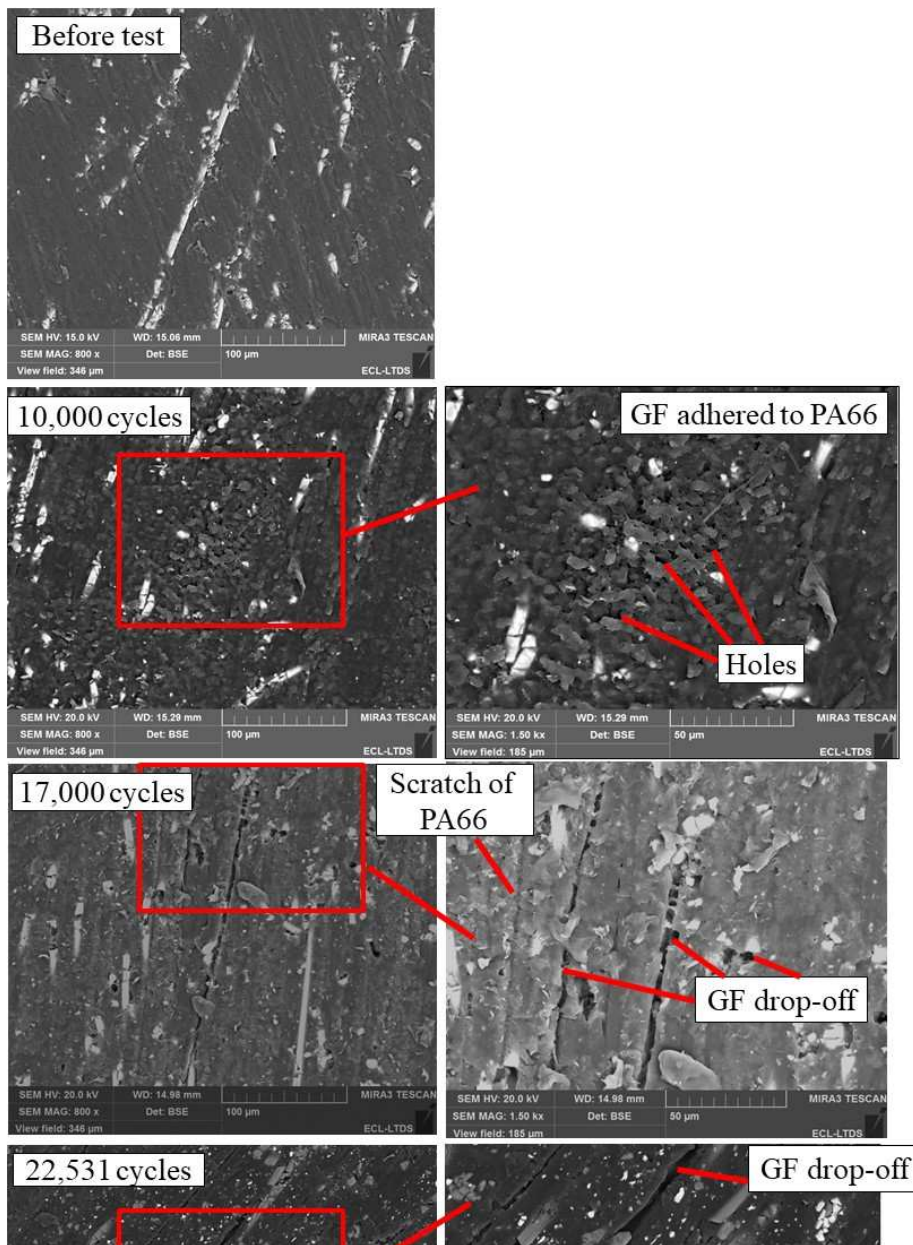


Fig. 10 SEM observations of the sliding surface of the composite after different numbers of cycles.

3.2 Wear behavior of counterpart steel and effect of the fiber orientation in the composite ring

The wear behavior of the counterpart steel cylinder was investigated. Figure 11 shows the wear volume of the steel cylinder for different cycles under the test conditions discussed in Section 3.1. Wear was measured by interferometry and corresponds to the total wear volume of the four cylinders. The wear volume increased proportionally with the number of cycles.

Figure 12 presents an optical microscope observation of a steel cylinder after 22,531 cycles (just before the first inflection point of the displacement), interferometric images of the cylinder before and after removal of the cylindrical shape for a better visualization of the wear, and a central longitudinal 2D profile measured through interferometry. The left area corresponds to the inner diameter side of the composite ring, and the right area corresponds to the outer diameter side of the composite ring. Severe wear of the steel cylinder, which appears to be 2-body abrasive wear, occurred even before the inflection point of the vertical displacement. This is related to the hardness of the steel and of the GF. The hardness of GF, which was measured by nano indentation, was approximately 5.7 GPa, and this value is much higher than the hardness of steel without heat treatment (4.50 GPa). Furthermore, the wear of the steel cylinder in the center area was much lower compared to the surface sides. This exhibits an inverse tendency to the wear of the composite ring, as discussed in Section 3.1. These results can be explained by the orientation of the GF in the composite as follows.

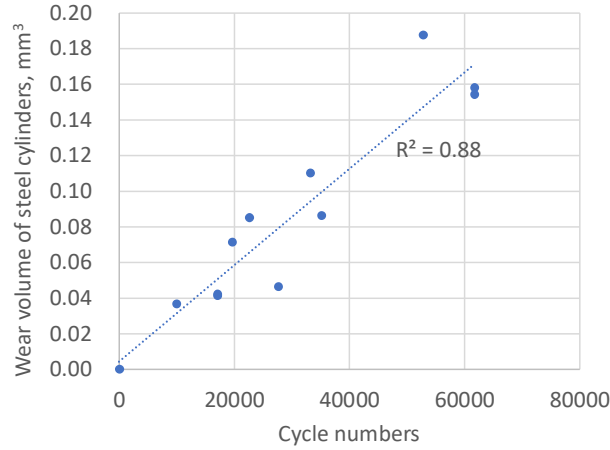


Fig. 11 Wear volume of steel cylinder for different sliding cycles.

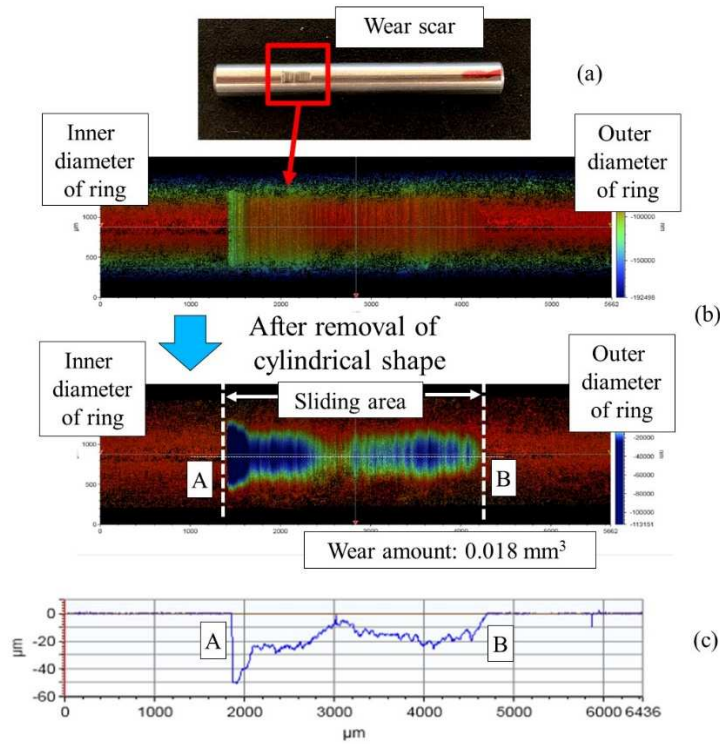


Fig. 12 Observation of steel cylinder after 22,531 cycles by (a) optical microscope and (b) 3D images of interferometry; (c) central longitudinal 2D profile measured through interferometry.

To better understand the differences in wear for each area of the steel, the differences in fiber orientation in the composite ring were evaluated quantitatively with an image analysis of the sliding surface of a composite ring. First, the polished sliding surface of the composite ring was prepared using #4000 polishing paper, and three BSE images of the inner/center/outer areas at a magnification of x300 were obtained, as shown in Figure 13. Afterward, the GF and PA66 areas were separated by binarization using the software package imageJ (produced by Wayne Rasband) as shown in Figure 14, and the total area of GF and the total perimeter of GF (corresponding to the total length of the contact between GF and PA66) were calculated. Furthermore, the distribution of the circularity of each GF was calculated. Circularity indicates the orientation of GF in the sliding

surface, and a value of circularity close to 1 means that the GF have a circular shape and are oriented in the perpendicular direction to the sliding surface. On the other hand, GF have a fibrous or oval shape when the value of the circularity decreases, indicating that the GF are oriented parallel to the sliding direction. Table 4 lists the calculated total area and total perimeter of GF in each area. Both values are similar in each area, therefore it is confirmed that the differences of the wear in the steel in each area are not attributed to the total area or perimeter of GF. Figure 15 presents the relationship between the circularity of the GF and cumulative area of GF, and Table 5 lists the average value of C_{50} in each area (C_{50} is the value of the circularity when the cumulative area of GF is 50%). The results indicate that the circularity in the center area is much lower than in the inner/outer areas, meaning that the majority of GF in the center area are aligned in parallel with the sliding direction. Therefore, the number of edges of GF which have much higher aggressive effects on the steel is lower, and wear in this area of the steel cylinder was much lower. In contrast, the GF can be easily peeled off because of the sliding shear stress; therefore, peeling of the composite material easily occurred. On the other hand, the circularity of the inner/outer areas is much higher than in the center area, therefore the GF are perpendicular to the contact surface. As a consequence, the wear on the steel cylinder is promoted because the number of edges of GF is much higher compared to the center area, and the wear of the composite ring is reduced.

The reason why the differences in GF orientation occurred can be explained as follows: inside the metal die during the injection molding process, the solidification speed is much higher in the inner and outer areas of the composite ring because these parts are in contact with the surface of the metal die, therefore the GF are oriented to the direction of resin flow. On the other hand, in the center area of the composite ring, the solidification speed is much lower because this area is not in contact with the metal die, therefore the GF flows before solidification occurs in the metal die.

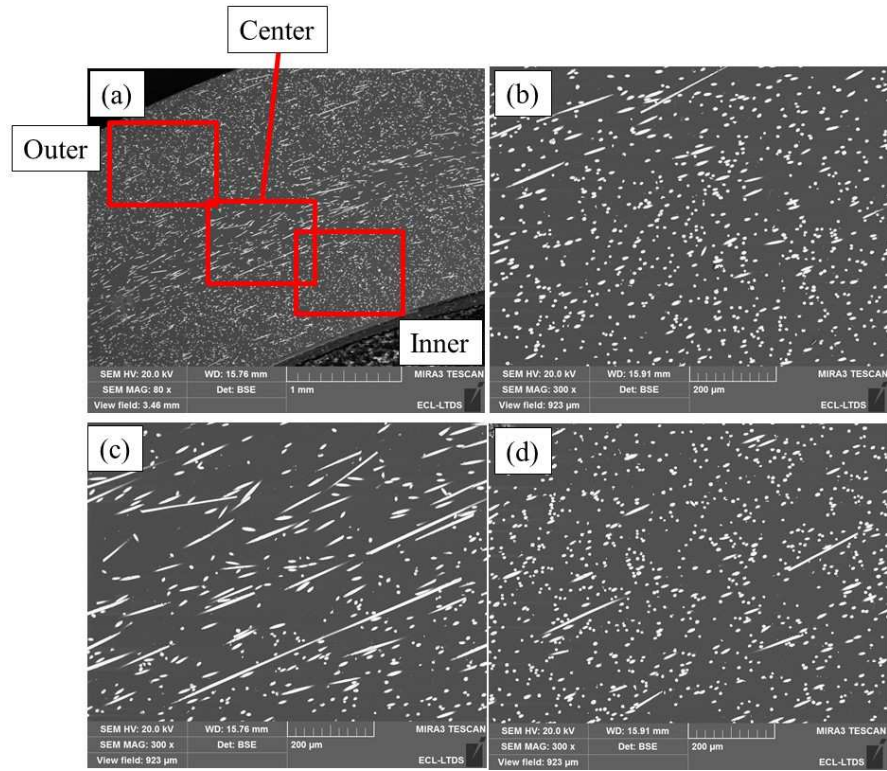


Fig. 13 SEM images of sliding surface of composite in each area

(a) Global view; (b) Inner area; (c) Center area; (d) Outer area



Fig. 14 Image analysis

(a) SEM image; (b) Binarization of image; (c) Particle analysis

Table 4 Calculated total area and total perimeter of GF in each area (Average value of different 3 positions).

Area	Area of GF in sliding surface	Total perimeter of GF
Inner area	8.4 +/- 0.1 %	25.3 +/- 1.0 mm
Center area	8.8 +/- 0.8 %	23.3 +/- 2.3 mm
Outer area	8.0 +/- 0.2 %	24.8 +/- 1.3 mm

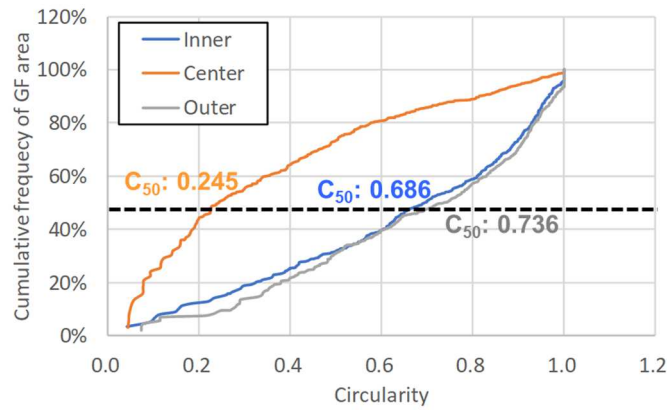


Fig. 15 Example of the relationship between the circularity of GF and cumulative area of GF

Table 5 Values of C_{50} (the circularity when the cumulative area of GF is 50%, the average value of different 3 positions).

Area	Values of C_{50}
Inner area	0.63 +/- 0.09
Center area	0.25 +/- 0.04
Outer area	0.73 +/- 0.07

3.3 Contribution of each parameter to the increase of friction and damage

The individual contributions of four parameters: the evolution of the sliding surface, the contamination of grease by wear debris, the wear of the steel cylinder, and the increasing sliding surface temperature were investigated by performing sliding tests under different conditions. Steel cylinders without heat treatment (hardness: 4.50 GPa) were used, and the same normal load and sliding speed as discussed in Section 3.1 were applied in all tests to clarify the contribution of each parameter separately.

First, the effect of the sliding surface damage was investigated. Pre-damaged composite rings after 17,000 cycles, 20,000 cycles, and 30,000 cycles were prepared, and sliding tests were performed using these pre-damaged rings under the same test conditions, using new steel cylinders and grease. Figure 16 presents the sliding surfaces before the sliding tests and the results of the sliding tests. The average friction coefficient becomes much higher with increased pre-damaged cycles. The temperature depends on the value of the friction coefficient, and a higher friction coefficient induces a greater increase of the temperature. In addition, the inflection point of the vertical displacement occurs much earlier with increased pre-damaged cycles. Considering these results, it is worth mentioning that the initial surface condition of the composite ring has a significantly strong effect on the increase in friction and therefore on the ultimate damage.

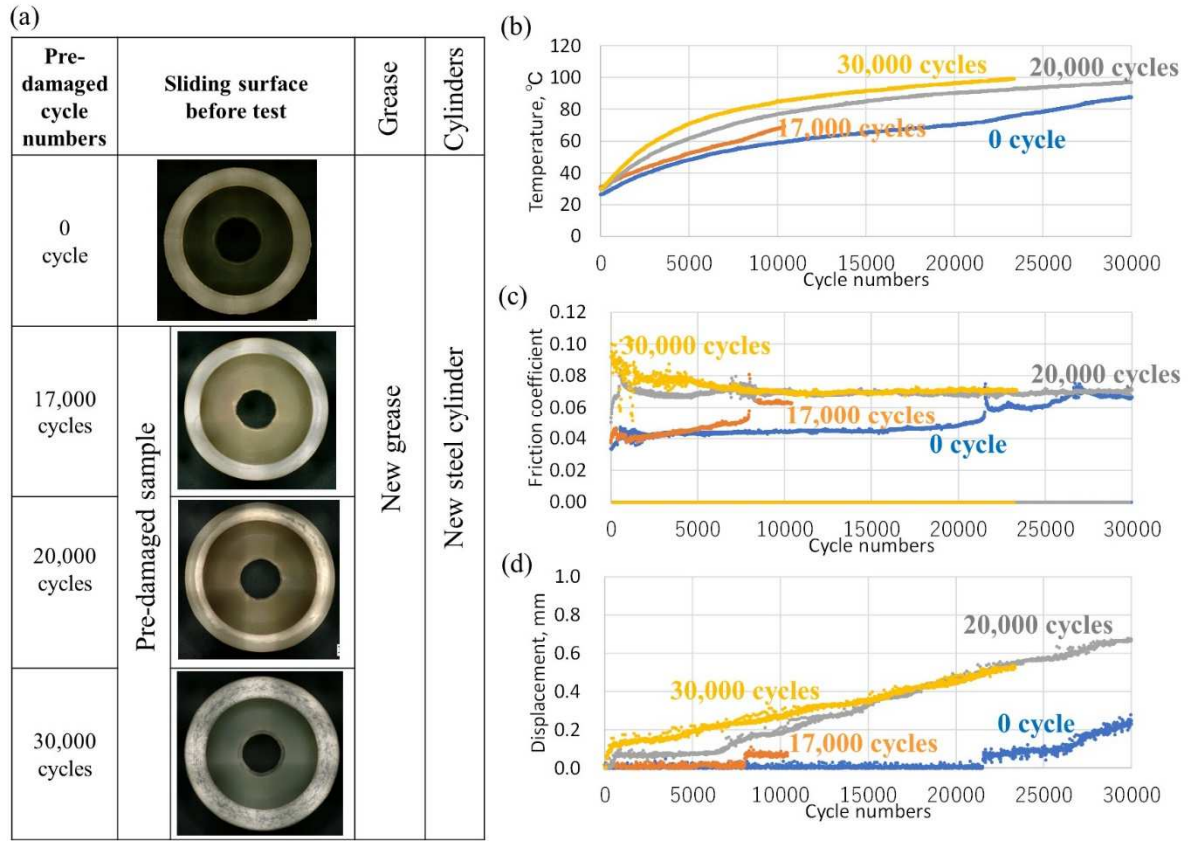


Fig. 16 (a) Sliding surface of pre-damaged composite rings before sliding tests; (b) evolutions of temperature; (c) evolutions of friction coefficient; (d) evolutions of displacement

The effect of the contamination of grease by wear debris on the friction and damage was investigated. After a sliding test of 61,500 cycles under the standard test conditions, grease was collected. This grease was contaminated by wear debris consisting of steel and GF, as explained in Section 3.1 (Figure 6). A new sliding test was then performed using this contaminated grease to compare the results when using new grease. Figure 17 presents the sample holder of a steel cylinder with the tested grease and the results of sliding tests. The sliding time evolution of the friction coefficient, temperature, and displacement were the same in both greases. In addition, the wear amount and morphology of the counterpart steel was also at the same level (with using new grease: 0.156 mm^3 , using the contaminated grease: 0.151 mm^3 in the total wear amount of four cylinders measured by interferometry) as presented in Figure. 18. Given these results, there is no effect of wear debris on the friction and wear of composite and steel. In addition, the wear mode of the steel is not 3-body abrasion; rather it is 2-body abrasion, because the wear debris of dropped off GF and steel which were present in the contaminated grease had no negative effects on the tribological properties of the contact, and wear of the steel is affected by the GF embedded in the PA66 when considering the wear scar of steel presented in Figure 5. Furthermore, the wear mode of the composite was also not 3-body abrasion, and the wear resistance of the composite is dominated by the damage to its sliding surface, as mentioned above.

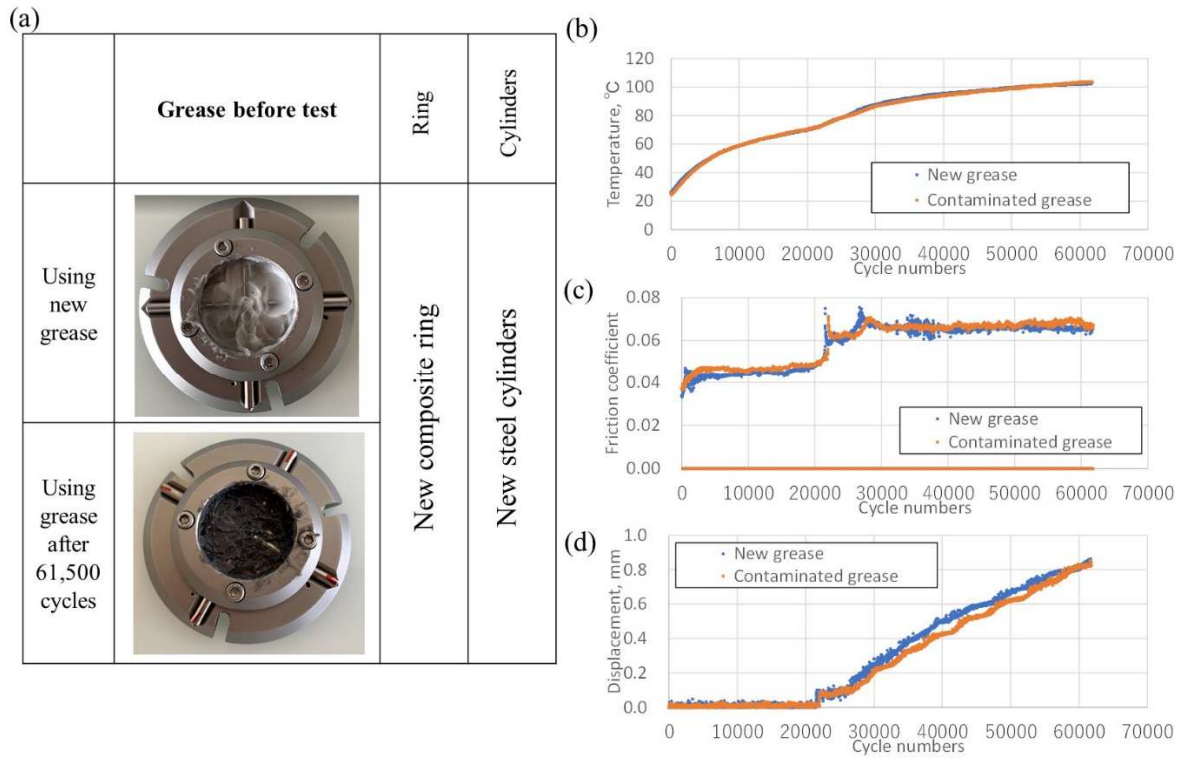


Fig. 17 (a) Grease in sample holder before sliding tests; (b) Evolutions of temperature; (c) Evolutions of friction coefficient; (d) Evolutions of displacement

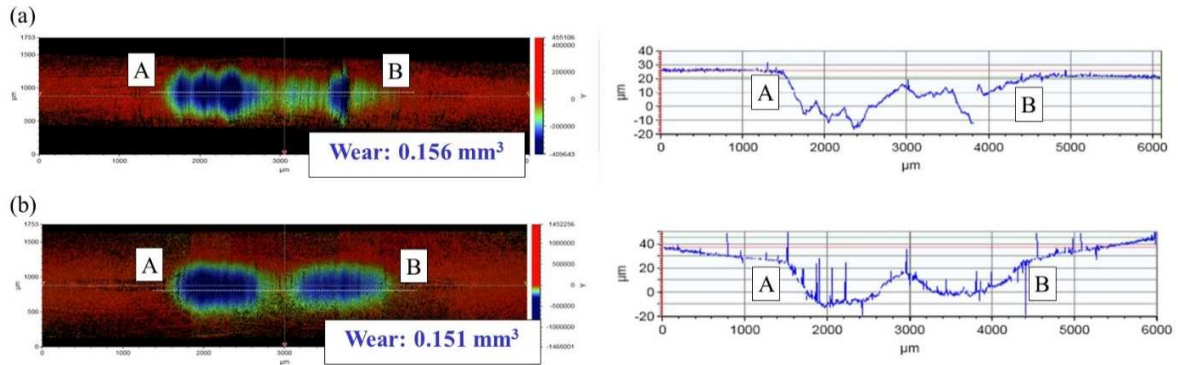


Fig. 18 Observation and central longitudinal 2D profile of counterpart steel after sliding test by interferometric measurement

(a) Using new grease; (b) using contaminated grease

The effect of the worn steel cylinder was also investigated. Pre-damaged steel cylinders after a 17,000 cycles sliding test were prepared, and a new sliding test was performed using these pre-damaged cylinders with new composite rings and grease. Figure 19 presents the steel cylinders before and after the sliding tests. The friction coefficient tends to decrease when using the pre-damaged steel cylinders compared to the results with new cylinders, and the temperature decreased. In addition, when using the pre-damaged steel cylinders, the inflection point of the vertical displacement occurs much later than when using new cylinders. The reason why using the pre-damaged steel cylinders improved the tribological properties appears to be a decrease of the contact pressure when using the worn cylinders. Therefore, the friction coefficient and temperature decreased, and wear

resistance was improved.

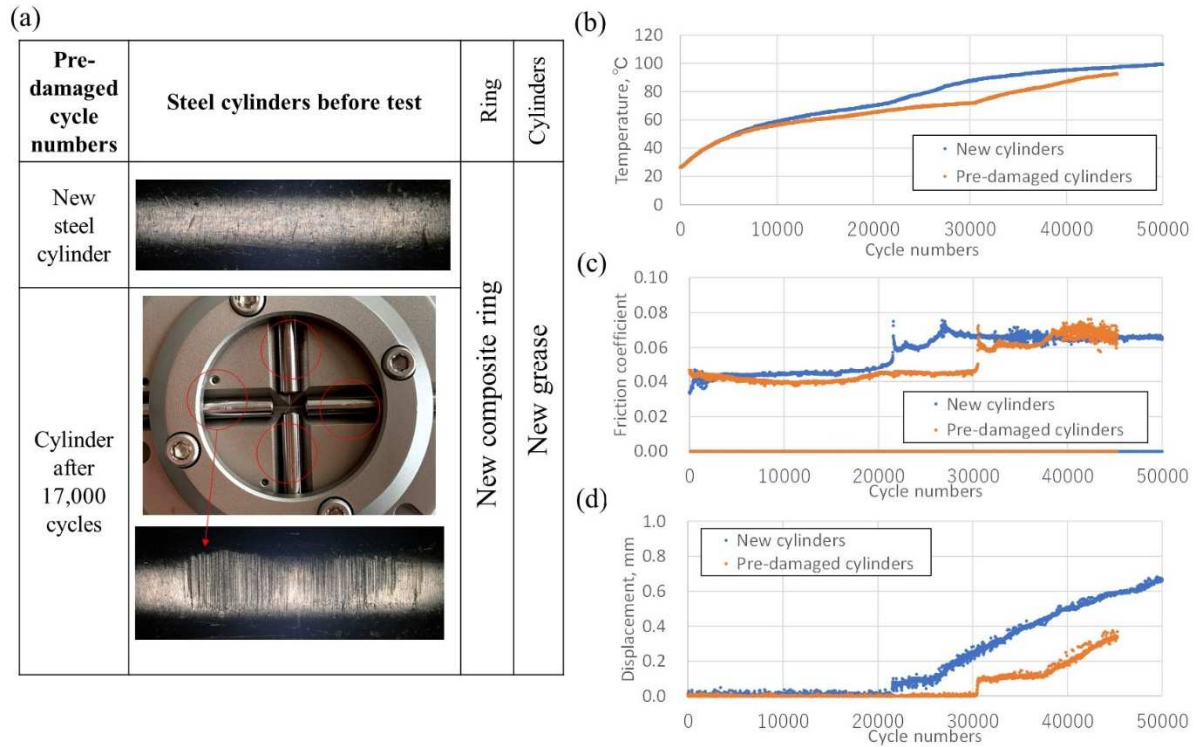


Fig. 19 (a) Sliding surface of a pre-damaged steel cylinder before sliding tests;
(b) Evolutions of temperature; (c) Evolutions of friction coefficient; (d) Evolutions of displacement

Additionally, the effect of the increase of temperature was investigated by performing sliding tests in which the test was stopped after 17,000 cycles and restarted once the temperature fell to room temperature. Figure 20 presents the test conditions: Test No. 1 used the normal test conditions without stopping after 17,000 cycles. In test No. 2, the sliding test was intentionally stopped after 17,000 cycles (before the inflection point of the vertical displacement) and the temperature decreased to room temperature (the normal load was removed to avoid creep during the cooling period), and the sliding test was restarted without changing the grease or steel cylinders. In test No. 3, the sliding test was stopped at the same number of cycles and the temperature was allowed to decrease under the same conditions, but the grease was replaced with new grease before restarting the sliding test. In test No. 4, steel cylinders were replaced with new ones; however, the grease was not changed before the restart of the sliding test after 17,000 cycles. Furthermore, in test No. 5, the grease and cylinders were both replaced after 17,000 cycles and the sliding test was restarted. Figs. 20 (b), (c), and (d) present these test results. Comparing the results of tests No. 1 and No. 2, the inflection point of the friction coefficient and vertical displacement occurs much later when the test is stopped after 17,000 cycles than when the test is not stopped. This is attributed to the recovery of the surface mechanical properties of the composite ring resulting from the decrease of the temperature; the tribological properties were improved compared to the continuous sliding condition. Thus, it can be stated that the increase in temperature deteriorates the tribological properties. Comparing the results of tests No. 2 and No. 3, very similar results were obtained, even if the grease was

replaced after the stop at 17,000 cycles in test No. 3, further verifying that there are no adverse effects due to contamination of wear debris in the grease, as mentioned previously. Comparing the results of tests No. 2 and No. 4, the inflection point of the friction coefficient and vertical displacement occurs much earlier in test No. 4 than in No. 2. This result is attributed to the increase in contact pressure that results after replacing the worn cylinders with new ones in test No. 4, as mentioned previously. In addition, comparing tests No. 4 and No. 5, the timing of the inflection points is the same. This is also attributed to the fact that contamination of the grease has no effect on the tribological properties, because the wear mode is not 3-body abrasion but is rather 2-body abrasion.

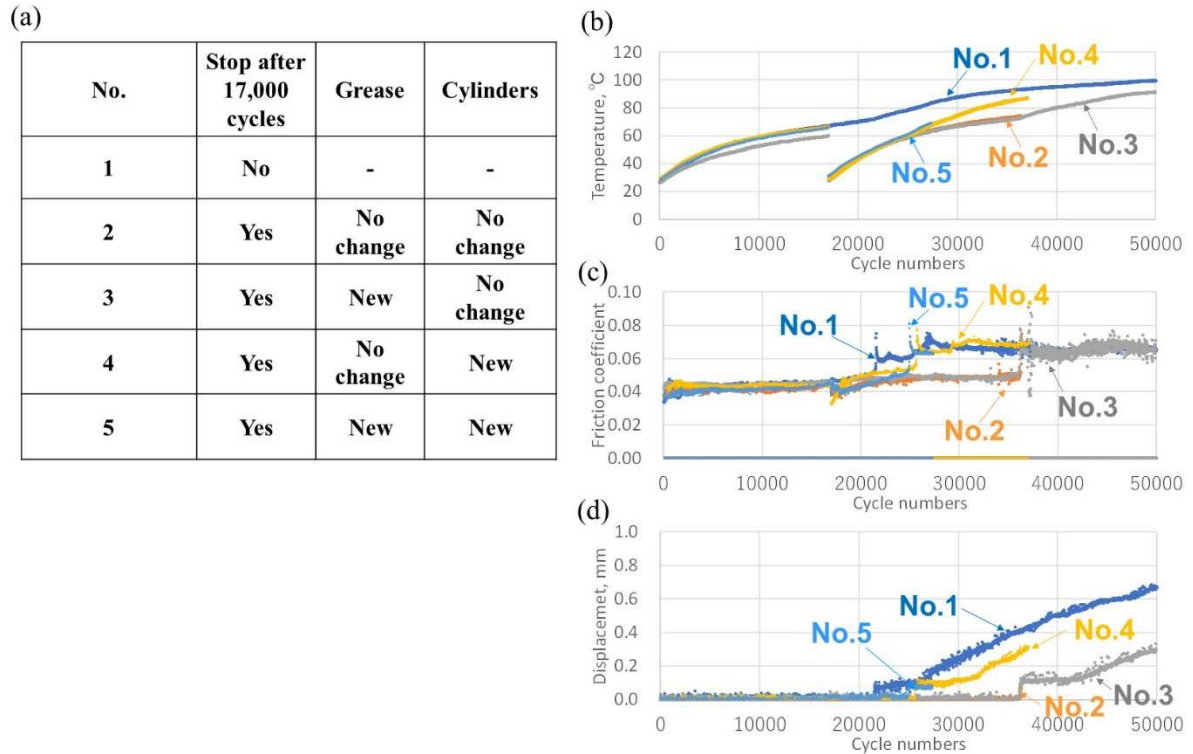


Fig. 20 (a) Test conditions; (b) Evolutions of temperature; (c) Evolutions of friction coefficient; (d) Evolutions of displacement

Consequently, the wear of the composite and particularly the linear increase in the vertical displacement are mainly dependent on the number of contact cycles and the contact pressure, and is less dependent on the contamination of the wear debris in grease or wear of the steel cylinder. Therefore, it would be possible to be concluded that the wear of the composite could be induced by contact fatigue, generating the maximum von-Mises stress below the contact surface, which can induce the peeling observed.

3.4 Effects of the hardness of the steel counterpart

The effects of the hardness of the counterpart steel cylinder on the tribological properties were investigated. Tests were performed with cylinders having different values of hardness (from 4.50 GPa to 9.89 GPa, measured by micro indentation). Total sliding cycles were 33,000 cycles. Figure 21(a) presents the estimated wear, creep, and total height loss of the composite ring for different values of steel cylinder hardness. The estimation of wear

and creep was performed in the same way as presented in Section 2.1. Figure 21(b) shows the wear volume of the counterpart steel cylinders for different values of hardness (total of the wear of four cylinders). Figure 22 presents the charts for each sliding test. Figure 23 presents microscope observation images of the sliding surface of a composite ring after the tests. It is observed that wear and creep of the composite increase with increasing hardness of the counterpart steel cylinders from 4.50 GPa to 5.36 GPa. On the other hand, wear is at the same level and the slope of the increase in creep decreases for hardness values ranging from 5.36 GPa to 7.81 GPa. Moreover, the timing of the inflection point of the friction coefficient and the vertical displacement occurs much earlier when using harder steel cylinders (from 4.50 GPa to 7.18 GPa), and sliding surface temperature is also increased. The evolution of the temperature, the friction coefficient, and the vertical displacement is the same between 7.18 GPa and 9.89 GPa. On the other hand, the wear of the counterpart steel cylinders sharply decreases with increasing hardness of the steel cylinders from 4.50 GPa to 5.36 GPa, and very little wear of steel is observed for hardness values ranging from 5.36 GPa to 7.81 GPa. A change in the color of the grease was not observed in this range.

These results are explained by the difference between the hardness of the GF and the counterpart steel cylinders. The hardness of GF was measured using the following process. First, the GF were embedded in epoxy resin in the horizontal or perpendicular direction, as presented in Figure 24(a), and the epoxy resin was cured. Then, the surface of the epoxy resin was polished and the hardness of the GF in each direction was measured using a nano indentation process; the normal load used for the measurements was 4,000 μN . Figure 24(b) shows the AFM images after the hardness measurements, and the indentations are observed on the surface of the GF. Figure 25 shows the load displacement curve for the measurements and the obtained hardness of the GF in each direction. No difference in hardness was observed between the horizontal and perpendicular directions, and the value was close to the hardness of steel with a hardness of 5.36 GPa.

Considering these results, it can be stated that when the hardness of the counterpart steel is significantly lower than the hardness of the GF, the wear of the composite and the damage to GF are reduced, while the aggressive effects of GF on the softer counterpart steel increase. In addition, the wear and creep of the composite decrease owing to the effects of the decreased contact pressure between GF and steel, which are related to the lower hardness of the steel. Furthermore, the large amount of wear on the counterpart steel induces a further decrease of the contact pressure, and wear and creep of the composite are also reduced. By contrast, wear and creep of the composite increased with increasing hardness of the counterpart steel because the aggressive effects of GF on the steel decreased, and the aggressive effects of the steel on the composite increased, as presented in Figs. 21(a) and (b). The contact pressure remains at a higher level because the wear on the steel cylinders decreased. In addition, the higher contact pressure between GF and steel related to much higher hardness of the steel increases the wear and creep of the composite.

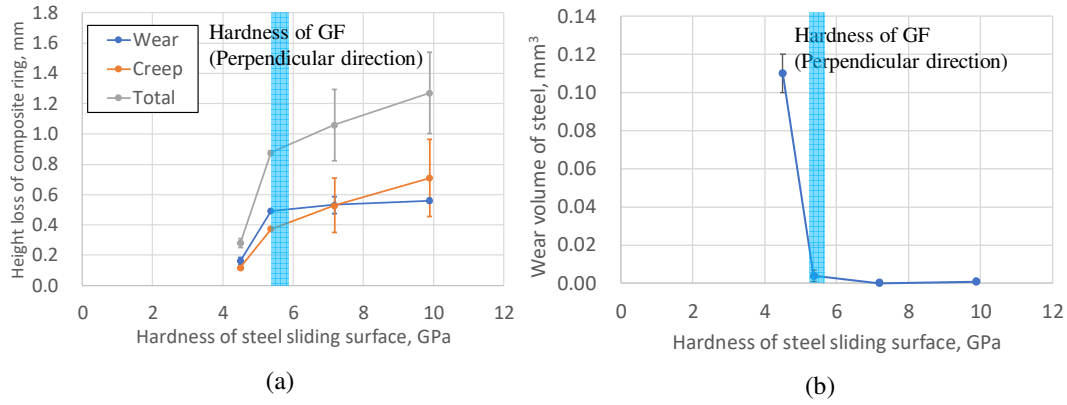


Fig. 21 (a) Wear, creep, and total height loss of composite ring for different hardness values of steel cylinders, as measured by micro indentation (average values of 2 measurements); (b) Wear volume of counterpart steel cylinder for different hardness values of steel cylinders, as measured by micro indentation (average values of 2 measurements).

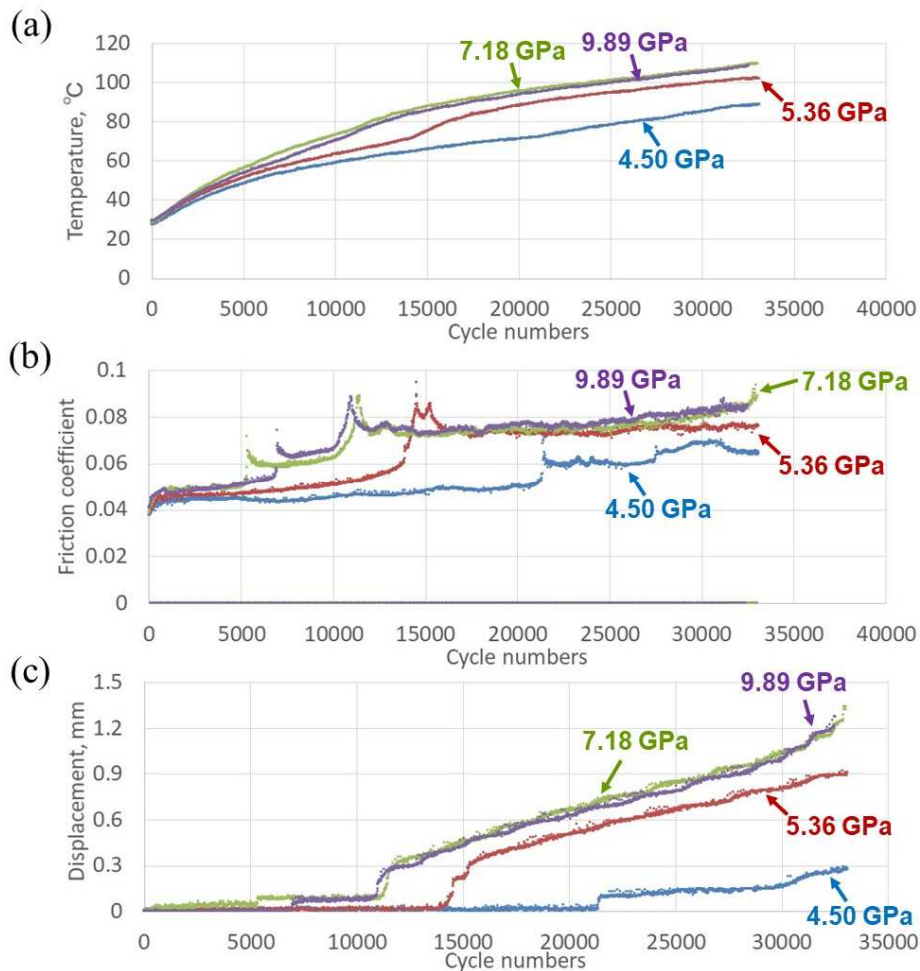


Fig. 22 Test charts for different values of hardness of steel cylinders;
(a) evolution of temperature; (b) evolution of friction coefficient; (c) evolution of displacement

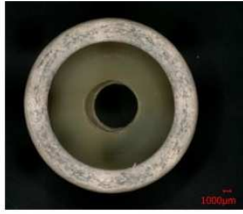
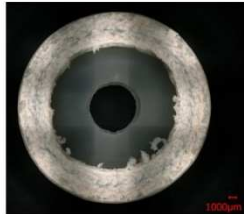
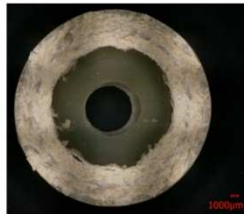
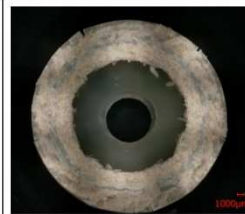
Hardness of steel	4.50 GPa	5.36 GPa	7.18 GPa	9.89 GPa
Composite ring sliding surface				

Fig. 23 Microscope observations of sliding surface of composite rings after tests using counterpart steel cylinders with different values of hardness.

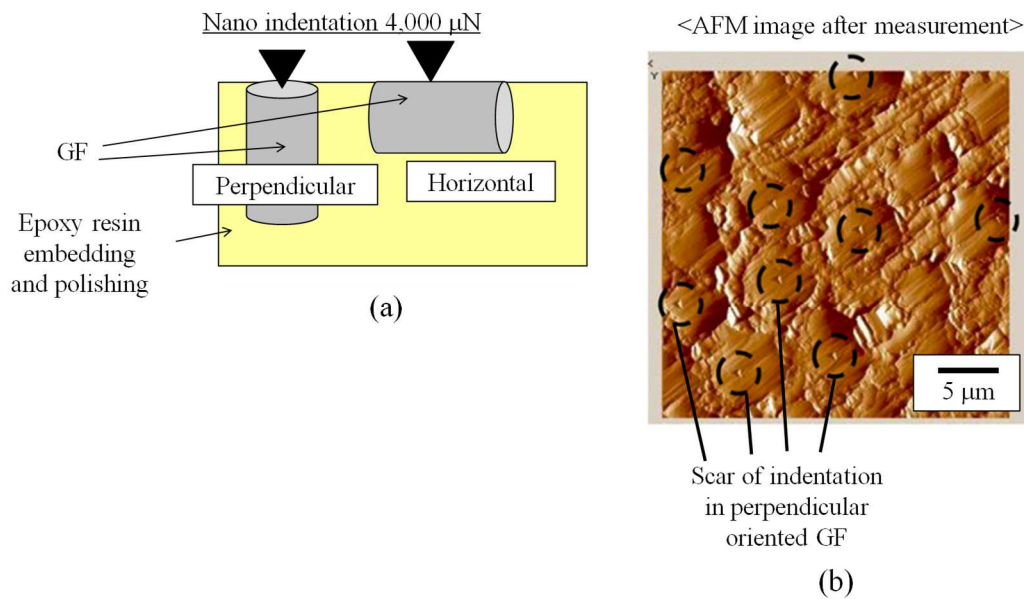


Fig. 24 (a) Measurement method of the hardness of GF using nano indentation and (b) AFM image of measured surface after measurements in the perpendicular direction.

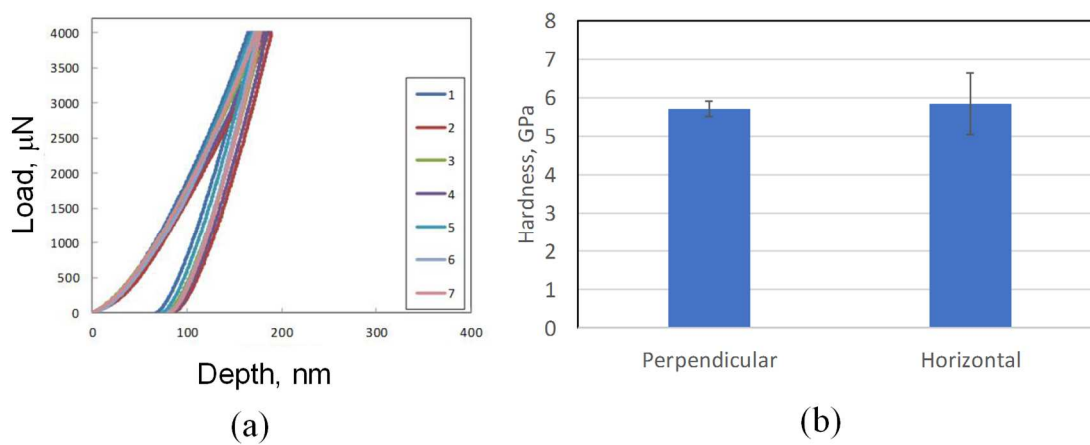


Fig. 25 (a) Load-displacement curves obtained using nano indentation measurements and (b) measured hardness of GF in each direction (average values in 7 measurements).

4. Conclusions

The tribological mechanisms of glass fiber-reinforced polyamide 66 material sliding in contact with a steel counterpart under high contact pressure in grease-lubricated conditions were clarified. The following points should be highlighted.

1) Detailed tribological behavior of the contact area and damage to the composite

An initial inflection point of the vertical displacement during sliding tests was observed and it was related to the creep of the composite ring. After this inflection point, the wear increased linearly with increasing number of cycles. The mechanical properties of the sliding surface change over time according to the damage inflicted on the sliding surface of the composite, and the damage to the sliding surface induces the increase of creep and friction coefficient.

2) Wear behavior of counterpart steel and the effect of the fiber orientation of the composite

An important effect regarding the fiber orientation on the sliding surface of the composite was observed on the wear resistance of the counterpart steel and composite. The aggressive effects observed on the counterpart steel were much greater when fibers were oriented in the perpendicular direction. By contrast, the wear of the composite increased when the fibers were aligned parallel to the sliding direction.

3) Contribution of each parameter on the increase of friction and damage

The damage to the sliding surface of the composite ring has an important effect. The contamination of the grease has no effect on the friction coefficient and damage. Friction and damage of the composite were reduced when worn steel was used, which is attributed to a decrease of the contact pressure. Damage on the composite ring decreased with decreasing temperature, which is attributed to the recovery of the mechanical properties of the composite once it cools .

4) Effects of the hardness of the counterpart steel

The relative hardness between the steel and fibers is important in understanding the wear induced in the steel and composite. The wear resistance of the composite improves when the hardness of the counterpart steel is lower, because aggressive effects on a composite that has harder fibers are reduced when the steel is softer, while the wear on a steel cylinder reduces the contact pressure.

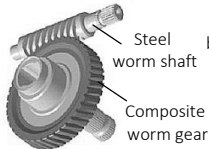
References

- [1] M. Kurokawa, Y. Uchiyama, S. Nagai, Performance of plastic gear made of carbon fiber reinforced polyether-ether-ketone: Part 2, *Tribol. Int.* 33 (2000) 715-721. [https://doi.org/10.1016/S0301-679X\(00\)00111-0](https://doi.org/10.1016/S0301-679X(00)00111-0)
- [2] R. J. Tappera, M. L. Longanaa, A. Nortonb, K. D. Pottera, I. Hamertona, An evaluation of life cycle assessment and its application to the closed-loop recycling of carbon fibre reinforced polymers, *Composite Part B* 184 (2020) 107665. <https://doi.org/10.1016/j.compositesb.2019.107665>
- [3] V. S. Balakrishnana, T. Hart-Rawungb, J. Buhl, H. Seidlitz, M. Bambachb, Impact and damage behaviour of FRP-metal hybrid laminates made by the reinforcement of glass fibers on 22MnB5 metal surface, *Composites Sci. and Technol.* 187 (2020) 107949. <https://doi.org/10.1016/j.compscitech.2019.107949>
- [4] R. Nakata, Grease lubrication technology for sliding automobile parts, *JTEKT Eng. J.* English Edition, 1011E (2014) 25–30.
- [5] S.M. Lee, M.W. Shin, H. Jangn, Effect of carbon-nanotube length on friction and wear of polyamide 6,6 nanocomposites, *Wear* 320 (2014) 103-110. <https://doi.org/10.1016/j.wear.2014.08.011>
- [6] M.T. Lates, R. Velicu, C.C. Gavrila, Temperature, pressure, and velocity influence on the tribological properties of PA66 and PA46 Polyamides, *Materials* 12 (20) (2019) 3452. <https://doi.org/10.33a90/ma12203452>
- [7] D.W. Gebretsadik, J. Hardell, B.P. rakash, Friction and wear characteristics of PA 66 polymer composite/316L stainless steel tribopair in aqueous solution with different salt levels, *Tribol. Int.* 141 (2020) 105917. <https://doi.org/10.1016/j.triboint.2019.105917>
- [8] J. Chen, H. Xu, C. Liu, L. Mi, C. Shen, The effect of double grafted interface layer on the properties of carbon fiber reinforced polyamide 66 composites. *Composites Sci. and Technol.* 168 (2018) 20-27. <https://doi.org/10.1016/j.compscitech.2018.09.007>
- [9] S. Senthilvelan, R. Gnanamoorthy, Damage Mechanisms in injection molded unreinforced, glass and carbon reinforced nylon 66 spur gears, *Appl. Compos. Mater.* 11 (2004) 377–397. <https://doi.org/10.1023/B:ACMA.0000045313.47841.4e>
- [10] B. Sarita, S. Senthilvelan, Effects of lubricant on the surface durability of an injection molded polyamide 66 spur gear paired with a steel gear, *Tribol. Int.* 137 (2019) 193–211. <https://doi.org/10.1016/j.triboint.2019.02.050>
- [11] S. Senthilvelan, R. Gnanamoorthy, Fiber reinforcement in injection molded nylon 6/6 spur gears, *Appl. Compos. Mater.* 13 (2006) 237–248. <https://doi.org/10.1007/s10443-006-9016-9>
- [12] J. Tavčar, G. Grkman, J. Duhovnik, Accelerated lifetime testing of reinforced polymer gears, *J. of Advanced Mec. Des., Sys., and Man.* 12 (2018) 1-13. <https://doi.org/10.1299/jamdsm.2018jamdsm0006>
- [13] Y. Zhang, C. Pursell, K. Mao, S. Leigh, A physical investigation of wear and thermal characteristics of 3D printed nylon spur gears. *Tribol. Int.*, 141 (2020) 105953. <https://doi.org/10.1016/j.triboint.2019.105953>
- [14] D. Scott, J. Blackwell, P.J. McCullagh, G.H. Mills, Composite materials for rolling bearing cages, *Wear* 15 (1970) 257-269. [https://doi.org/10.1016/0043-1648\(70\)90016-5](https://doi.org/10.1016/0043-1648(70)90016-5)
- [15] H. Oh, M.H. Azarian, C. Morillo, M. Pecht, E. Rhem, Failure mechanisms of ball bearings under lightly

- loaded, non-accelerated usage conditions, Tribol. Int. 81 (2015) 291–299. <https://doi.org/10.1016/j.triboint.2014.09.014>
- [16] J. Kohout, Strength changes of moulded polyamide composite caused by thermal oxidation, J. of Mat. Sci. 34 (1999) 843–849. <https://doi.org/10.1023/A:1004593417901>
- [17] M. Harrass, K. Friedrich, A.A. Almajid, Tribological behavior of selected engineering polymers under rolling contact. Tribol. Int. 43 (2010) 635–646. <https://doi.org/10.1016/j.triboint.2009.10.003>
- [18] M. Bondy, W. Rodgers, W. Altenhof, Tensile fatigue characterization of polyamide 66/carbon fiber direct/in-line compounded long fiber thermoplastic composites. Composites Part B: Eng. 173 (2019) 106984. <https://doi.org/10.1016/j.compositesb.2019.106984>
- [19] J.H. Fonseca, G. Han, L. Quagliato, Y. Kim, J. Choi, T. Keum, S. Kim, D.S. Han, H. Lee, Design and numerical evaluation of recycled-carbon-fiber-reinforced polymer/metal hybrid engine cradle concepts, Int. J. of Mec. Sci. 163 (2019) 105115. <https://doi.org/10.1016/j.ijmecsci.2019.105115>
- [20] G.H. Kim, J.W. Lee, T.II. Seo, Durability characteristics analysis of plastic worm wheel with glass fiber reinforced polyamide, Materials 6 (2013) 1873–1890. <https://doi.org/10.3390/ma6051873>
- [21] H. C. Ahn, Wear of glass fiber reinforced polyamide worm gear according to the direction of the glass fiber, Technical paper presented at SAE 2010 World Congress & Exhibition. <https://doi.org/10.4271/2010-01-0917>
- [22] A. Bormuth, J. Zuleeg, C. Schmitz, R. Schmitz, M. Pfadt and H. Meven, Lubrication of plastic worm gears, Power Transmission Eng. Aug. (2019) 42–47.
- [23] T. Kunishima, K. Miyake, T. Kurokawa, H. Arai, Clarification of tribological behavior on tooth surface of resin worm gear for electric power steering, JTEKT Eng. J. English Edition, 1013E (2016) 27–33.
- [24] S.N. Kukureka, C.J. Hooke, M. Rao, P. Liao, Y. K. Chen, Effect of fibre reinforcement on the friction and wear of polyamide 66 under dry rolling-sliding contact, Tribol. Int. 32 (1999) 107–116. [https://doi.org/10.1016/S0301-679X\(99\)00017-1](https://doi.org/10.1016/S0301-679X(99)00017-1)
- [25] S. Zhou, Q. Zhang, C. Wu, J. Huang, Effect of carbon fiber reinforcement on the mechanical and tribological properties of polyamide6/polyphenylene sulfide composites, Mater. Des. 44 (2013) 493–499. <https://doi.org/10.1016/j.matdes.2012.08.029>
- [26] D.H. Gordon, S.N. Kukureka, The wear and friction of polyamide 46 and polyamide 46/aramid-fibre composites in sliding-rolling contact, Wear 267 (2009) 669–678. <https://doi.org/10.1016/j.wear.2008.11.026>
- [27] S. S. Kim, M. W. Shin, H. Jang, Tribological properties of short glass fiber reinforced polyamide 12 sliding on medium carbon steel, Wear 274–275 (2012) 34–42. <https://doi.org/10.1016/j.wear.2011.08.009>
- [28] M.W. Shin, S.S. Kim, H. Jang, Friction and wear of polyamide 66 with different weight average molar mass, Tribol. Lett. 44 (2011) 151–158. <https://doi.org/10.1007/s11249-011-9833-3>
- [29] J.W. Kim, H. Jangn, Jin Woo Kim, Friction and wear of monolithic and glass-fiber reinforced PA66 in humid conditions, Wear 309 (2014) 82–88. <https://doi.org/10.1016/j.triboint.2019.105917>
- [30] M. Kurokawa, Y. Uchiyama, T. Iwai, S. Nagai, Performance of plastic gear made of carbon fiber reinforced polyamide 12, Wear 254 (2003) 468–473. [https://doi.org/10.1016/S0043-1648\(03\)00020-6](https://doi.org/10.1016/S0043-1648(03)00020-6)
- [31] M. Kurokawa, Y. Uchiyama, S. Nagai, Performance of plastic gear made of carbon fiber reinforced poly-ether-ether-ketone, Tribol. Int. 32 (1999) 491–497. [https://doi.org/10.1016/S0301-679X\(99\)00078-X](https://doi.org/10.1016/S0301-679X(99)00078-X)

- [32] T. Kunishima, T. Kurokawa, H. Arai, V. Fridrici, P. Kapsa, Reactive extrusion mechanism, mechanical and tribological behavior of fiber reinforced polyamide 66 with added carbodiimide, *Mater. Des.* 188 (2020) 108447. <https://doi.org/10.1016/j.matdes.2019.108447>
- [33] Y.K. Chen, O.P. Modi, A.S. Mhay, A. Chrysanthou, J.M. O'Sullivan, The effect of different metallic counterface materials and different surface treatments on the wear and friction of polyamide 66 and its composite in rolling-sliding contact, *Wear* 255 (2003) 714–721. [https://doi.org/10.1016/S0043-1648\(03\)00054-1](https://doi.org/10.1016/S0043-1648(03)00054-1)

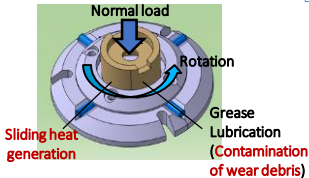
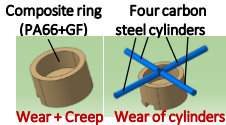
Composite sliding parts in contact with steel under grease lubrication



<Worm reducer>

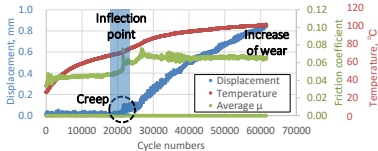
- High contact pressure
- High sliding speed
- Higher effect of sliding
- Grease lubrication

Simulation
by basic test



-Clarification of tribological behavior
and contribution of **each phenomenon**

<Evolution of displacement, T, μ >



<Effect of hardness of counterpart steel >

